Molecular Dynamics Insights into the Structural and Water Transport Properties of a Forward Osmosis Polyamide Thin-Film Nanocomposite Membrane Modified with Graphene

Molecular Dynamics Insights into the Structural and Water Transport Properties of a Forward Osmosis Polyamide Thin Film Nanocomposite Membrane Modified with Graphene Quantum Dots

Saeed Khoshhal Salestan[1, a], S. Fatemeh Seyedpour[1, a], Ahmad Rahimpour[a,c,d*], Ahmad Arabi Shamsabadi[b], Alberto Tiraferri[c], and Masoud Soroush[b*]

[a] Department of Chemical Engineering, Babol Noshirvani University of Technology, Babol, 4714781167, Iran

[b] Department of Chemical and Biological Engineering, Drexel University, Philadelphia, Pennsylvania 19104, United States

[c] Department of Environmental, Land and Infrastructure Engineering, Politecnico di Torino, C.so Duca degli Abruzzi 24, 10129, Turin, Italy

[d] Department of Applied Science and Technology, Politecnico di Torino, Corso Duca degli Abruzzi 24, 10129, Turin, Italy

Submitted for Publication in *Industrial & Engineering Chemistry Research*

Abstract

[*]Corresponding author: ahmadrahimpour@nit.ac.ir, ahmad.rahimpour@polito.it

[*]Corresponding author: soroushm@drexel.edu

[1]The authors contributed equally to this work

An approach combining molecular dynamics simulations and laboratory experiments was applied to provide new theoretical insights into the chemical structure of polyamide (PA) thin-film composite (TFC) membranes modified with graphene quantum dots (GQDs). The interaction energies, fractional free-volumes, mean-square displacements, densities, and water diffusion coefficients were computed for PA and four likely chemical structures of the GQDs-embedded PA membranes. These theoretical results aided with experimentally-measured water fluxes allowed for determining the most likely structure of the GQD-PA membrane. The compatibility of the GQDs and PA chains was found to be due to the formation of hydrogen and covalent bonds to m-phenylenediamine units. The modified membrane has a higher water diffusivity but a lower overall free volume, compared to the pristine PA membrane. MD simulations in concert with laboratory experiments were found to provide a good understanding of the relationship between microscopic characteristics and macroscopic transport properties of TFC membranes.

1. Introduction

Due to their excellent chemical stability as well as high rejection of salts and other dissolved contaminants, [1] polyamide (PA) thin-film composite (TFC) membranes are applied widely in desalination and forward osmosis (FO) processes. [2,3] The performance of these membranes depends strongly on their structure and physiochemical properties. [4,5] Extensive experimental studies have been carried out to fabricate PA FO membranes with a high water flux and a high salt rejection. [6–8] To improve and tailor the membrane properties, numerous types of nanomaterials have been incorporated into the PA selective layer. [9,10] However, this incorporation leads to improved complexity of the membrane structure of the membranes, which often prevents a rationalization of their final performance.

The physical properties of a PA layer that influence water and salt permeabilities include polymer composition, [11] molecular structure, [12] fractional free-volume (FFV), [13] and surface electric potential. [14] The functional groups of a PA membrane also have a significant effect on the water transport. [15,16] For example, hydroxyl and carboxyl functional groups have affinity to water molecules, and increasing the density of these moieties improve the water adsorption capacity of the membrane. [2,17] When a nanocomposite membrane is fabricated by incorporating nanomaterials into the membrane selective layer, the interfacial regions between PA chains and the filler affect the transport properties of the resulting membrane, especially the modifying materials have high density of surface functional groups.

Graphene quantum dots (GQDs) have appealing characteristics for membrane functionalization, such as large surface area and tunable surface grafting thanks to the presence of functional surface groups. [18–20] Specifically, the presence of hydroxyl and carboxyl functional groups on the surface of GQDs improves their compatibility with various polymeric,

63 organic/inorganic, and biological species. [21–23] Due to the presence of oxygen-containing
64 moieties, the incorporation of GQDs into the PA matrix alters its physiochemical structure, and
65 thus its water transport mechanisms. To develop nanocomposite PA membranes with suitable
66 performance, better understandings of the microscopic structure of the membranes and of the
67 interactions between PA chains and nanomaterials are needed. [2] As current experimental
68 methods are largely inadequate to provide insights into how the transport properties of PA
69 membranes are related to their microscopic structure, robust theoretical methods such as
70 molecular dynamics (MD) are appealing. [24]

71 MD studies have shown that the incorporation of nanoparticles into PA changes the
72 cross-linking degree of the PA network, significantly altering the water flux of the resulting
73 membranes. [25,26] It has been reported that MD can reliably predict the interfacial interactions
74 between fillers and the polymer matrix at the molecular level. [27–29] MD can also be applied to
75 elucidate the function of the filler functional groups and has provided a deeper insight into the
76 transport of water molecules through the structure of traditional PA membranes. [25] Overall, MD
77 simulation provides an improved understanding of the relationship between macroscopic
78 membrane transport properties and microscopic membrane properties, such as polymer
79 configuration and free volume distribution. [30,31] Previous MD studies have focused on the water
80 transport within PA membranes, [32,33] but they have not evaluated the effect of filler-polymer
81 interactions on membranes transport properties. Experimentally, it has been shown that
82 functionalization of carbon nanotubes (CNTs) can enhance their compatibility with polymeric
83 matrix, [34] and that embedding CNTs into PAs alters the performance of the resulting
84 nanocomposite membranes. [35,36] There have been a few MD studies on the effects of
85 incorporating CNTs into PA. These include investigations on the structure and hydration

properties of a CNTs/PA-TFC membrane, [37] the effect of interfaces on the structural and dynamical properties of CNTs/PA-66, [38] and the effect CNTs functionalization on the mechanical properties of the CNTs/chitosan nanocomposites. [39]

In this study, MD is applied to understand how the incorporation of GQDs into the PA matrix affect the molecular-scale interactions and to evaluate their effects on the water flux behavior of the resulting PA-GQDs membranes. To this end, the PA and GQDs structures are first constructed and they then placed in a cubic amorphous cell. Afterwards, the potential sites for the formation of covalent and hydrogen bonds on the PA chain are identified, and full MD simulations are conducted by binding GQDs to these sites. Considering the possible sites, different structures of the PA-GQDs membranes are created and then investigated. For all the PA and PA-GQDs structures, the interaction energies, density, fractional free-volume, mean square displacement, and water diffusivity coefficients are calculated. Based on these predictions and water flux data obtained from experiments, the most probable structure of the final nanocomposite matrix is determined, providing insights into the rationalization of the transport properties as a function of the nanoscale membrane structure.

2. Materials and Methods

2.1. Fabrication of the membranes

The PES membrane substrates were fabricated by the conventional phase inversion technique. [40,41] The casting solution containing polyethersulfone beads (PES 14 wt.%, Ultrason E6020P, M_w = 58,000 g/mol), polyvinylpyrrolidone (PVP 1 wt%, M_w = 25,000 g/mol, Merck), and Triton X-100 (2 wt%, Merck) was stirred in N,N-dimethylformamide (DMF, 99.5%, Scharlau) for at least 10 h to form a completely homogenous solution. After keeping the solution

stagnant for 6 h to eliminate entrapped bubbles, it was casted on a glass plate using a casting knife set at a gate height of 90 μm. The casted film was then immersed into a coagulation bath of deionized water (DI) and 1 wt/v % SDS.

GQDs were prepared by direct pyrolysis of citric acid (CA, Merck) according to the procedure previously reported in Ref.[42,43] The pristine and the GQDs-functionalized TFC membranes were prepared based on the procedure reported in our previous paper. [41] Briefly, polyamide layers of all neat TFC and thin-film nanocomposite (TFN) membranes were fabricated by interfacial polymerization (IP) between 3-phenylendiamine (MPD, Merck) (2 min) and trimesoylchloride (TMC, Merck) TMC (30 s) solutions on the PES substrate**.** The aqueous solution contained 2 wt% MPD, 2 wt% Camphorsulfonic acid (CSA, Merck) and 1 wt% Triethylamine (TEA, Merck), while the organic solution included 0.1 wt/v% TMC in n-hexane (96%, scharlau)**.** After sequential immersion into aqueous and organic solutions, the polyamide membrane was subjected to post-treatment in an oven at 80 °C for 5 min to ensure complete cross-linking between monomers. [44] The TFN membranes were fabricated via incorporating GQDs (0.05, 0.1, 0.3 and 0.5 wt.%) into the aqueous solution during the IP process, in which the GQDs were distributed in the MPD solution using ultra-sonication.

It is worth mentioning that as this study focused on the characteristics of the selective layer of polyamide membranes, the support layer was not considered during simulations. Hereafter, the resulting membranes are denoted as thin-film nanocomposite (TFN)-0.05, TFN-0.1, TFN-0.3 and TFN-0.5, respectively.

2.2. Membrane water flux measurement

The water flux (J_w) of the TFC and TFN membranes were determined by a lab-scale cross-flow FO unit with an active area of 30 cm^2 and an active layer in the feed side. A closed-

loop configuration with the aid of two gear pumps was applied to circulate the feed and draw solutions. [40] In all experiments, DI water was used as the feed, and sodium chloride (NaCl, 99.5% Merck) with a concentration of 0.5 M NaCl was used as the draw solution. Each experiment was conducted for 30 min and was repeated three times. Conductivities of the feed and draw solutions were measured online using a bench-scale conductivity meter (AZ86503). The change of mass in feed solution was determined by a digital balance (AND EK6000I) connected to a computer. The FO water flux (Jw) was then calculated via the following equation:

$$J_w = -\frac{\Delta(m_{fs} \times y_w)}{\Delta t} \times \frac{1}{\rho_w A_m} \quad (1)$$

where m_{fs}, ρ_w, and y_w are the mass of the feed solution, the pure-water density, and the mass fraction of water in the feed solution, respectively. A_m is the effective membrane area. $\Delta(m_{fs} \times y_w)$ is the change in term $(m_{fs} \times y_w)$ over a time interval of Δt.

2.2. Simulation methodology

All the molecular dynamics (MD) simulations were performed with Materials Studio 6 (MS) software (Accelrys Inc., San Diego). To simulate likely interactions of hydroxyl- and carboxyl-functionalized GQDs with polyamide chains, the following five different structures were considered:

- P1: A neat polyamide chain formed by the reaction of TMC and MPD.
- P1-GQD: A mixture of P1 and three non-bonded GQDs.
- P2-GQD: A mixture of two non-bonded GQDs and one functionalized P1 with GQDs (one GQD is connected to an MPD unit of the P1 monomer).

- P3-GQD: A mixture of two non-bonded GQDs and one functionalized P1 with GQDs (GQDs are connected to several MPD and TMC units of the P1 monomer).
- P4-GQD: A mixture of two non-bonded GQDs and a functionalized P1 with GQDs (one GQD is connected to a TMC unit of the P1 monomer).

The structures of GQD and the repeat units of P1, P2-GQD, P3-GQD and P4-GQ, are illustrated in Figure 1. 3D atomic models of GQD and the monomers depicted in Fig. 1 are provided in the Supporting Information. The files, GQD, Amid-1, Amid-2, Amid-3, and Amid-4, correspond to the structures provided in Fig. 1a-e, respectively. Moreover, Figure 2 shows the interfacial polymerization reaction of TMC and MPD to form a PA chain, as well as the interaction mechanisms of GQDs with MPD and TMC units proposed in previous studies. [41,45]

Xu et al. [46] proposed a reaction mechanism, in which the formation of covalent bonds between amine species (polyethylenimine) and GQDs is more probable than the reaction between GQDs and TMC units. In this study, we investigate this mechanism and three more likely ones described above.

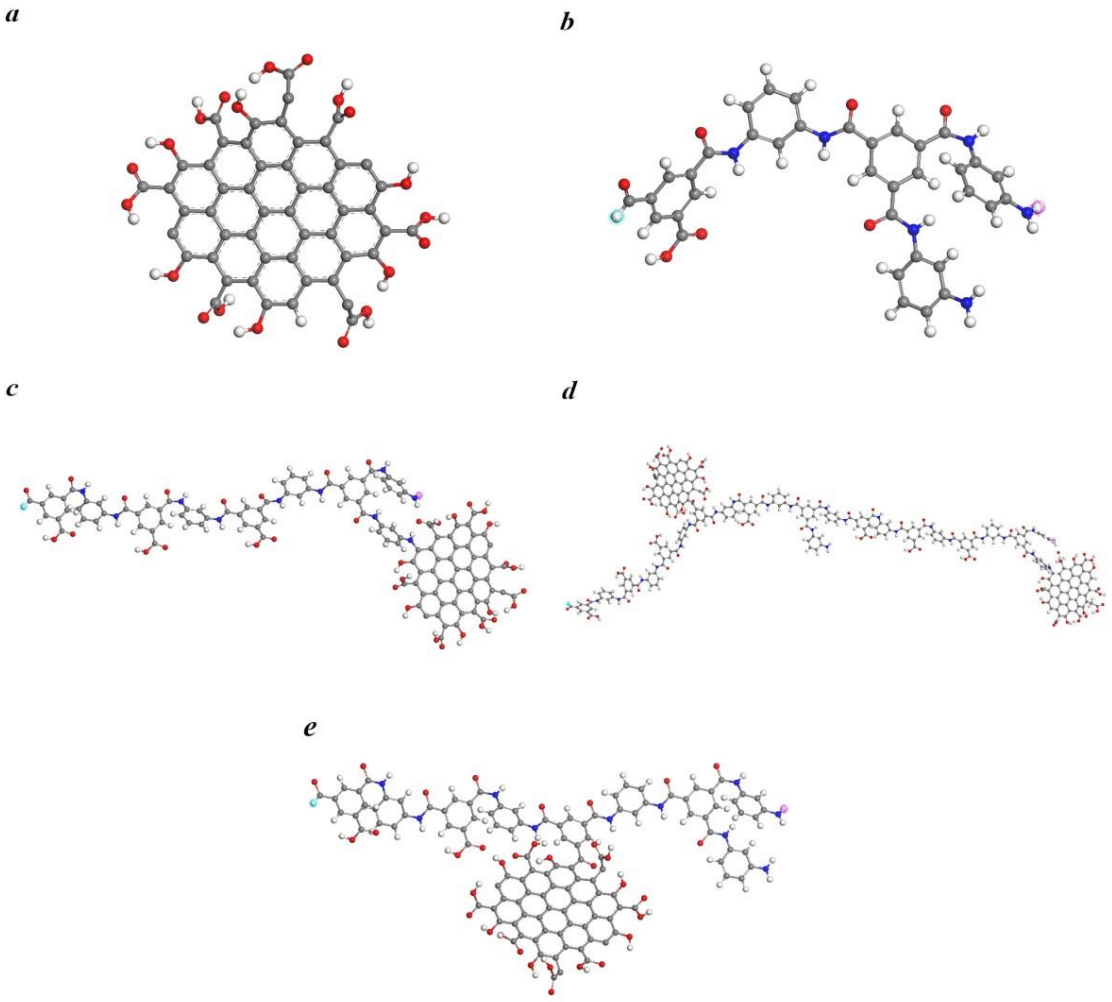

Figure 1: Chemical structures of (a) GQD and the other monomer structures used in (b) P1, (c) P2-GQD, (d) P3-GQD, and (e) P4-GQD samples, respectively

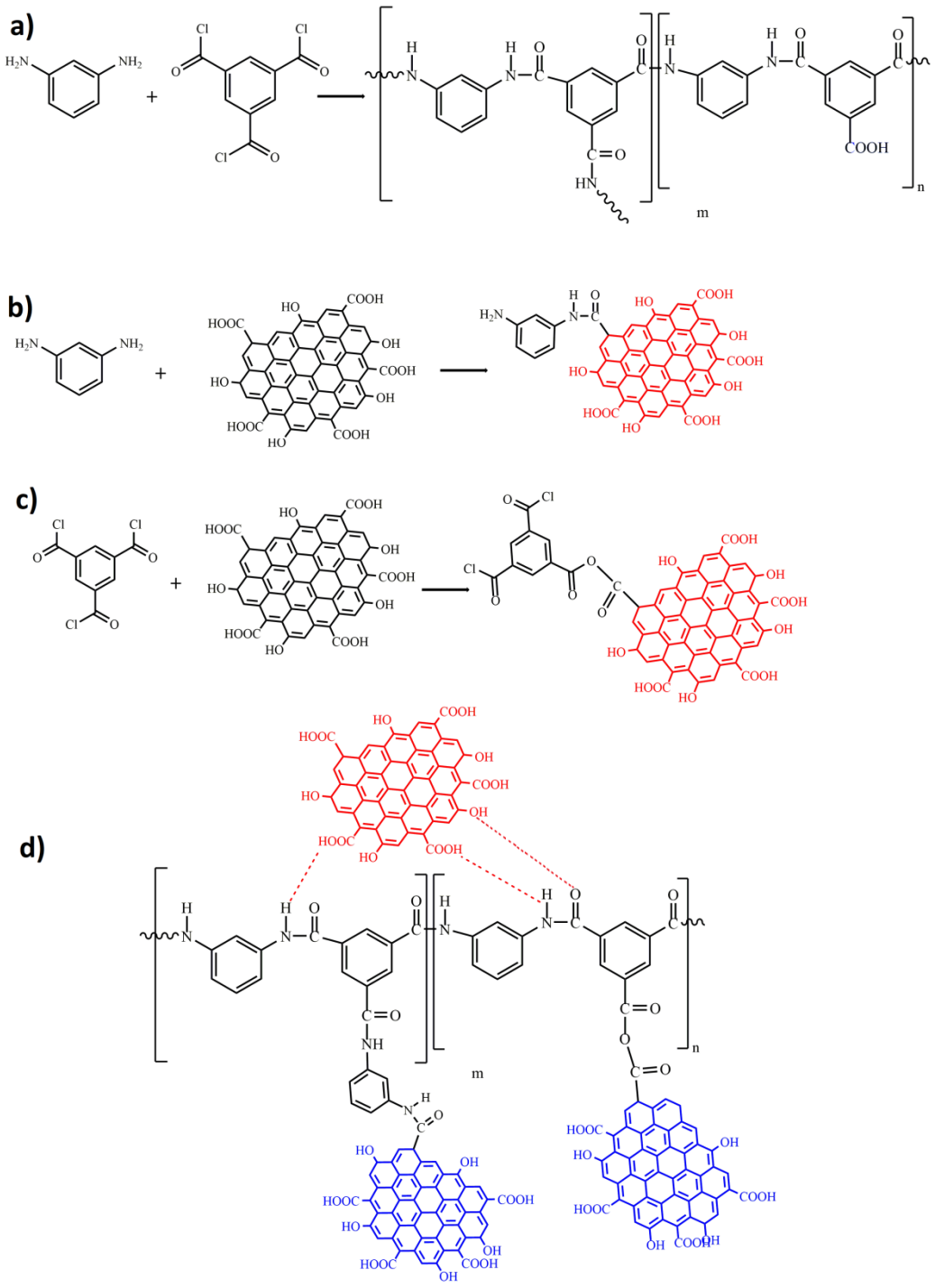

171

172 **Figure 2.** a) Interfacial polymerization between a TMC and an MPD unit, b) the interaction between a
173 GQD and an MPD unit, c) the interaction between a GQD and a TMC, and d) the hydrogen bonds
174 between GQDs and a PA chain and the formed covalent bonds between GQDs and both MPD and TMC
175 units in a PA chain proposed in previous studies. [41,45]

176

The structures of P1 and GQDs were connected by deploying the 'Homopolymer Builder Module'. The initial model of the membranes was developed based on the proposed structures constructed under periodic boundary conditions in the "Amorphous Cell" module. The lattice type of the cells was adjusted as cubic and their initial densities were set at 0.1 g/cm^3. One chain of each proposed structure was included in the simulation cell and its molecular weight was set around 10,000 g/mol. Using the 'Forcite Module' and the 'Smart Minimizer' function, all the structures were optimized in terms of both geometry and energy.

Two sets of simulations were conducted to study the properties of the four different structures. One set investigated the intramolecular interactions between the GQDs and PA chains in terms of covalent and hydrogen bonds, while the second set evaluated the water diffusivity by loading water molecules within the amorphous cells. At each simulation stage, the periodic boundary conditions (PBC) method was implemented to avoid undesirable interactions of the molecules with the walls of the amorphous cell. An energy minimization procedure was applied to find the equilibrated structure with the minimum potential energy for the amorphous cells. To obtain equilibrium structures and true densities, MD simulations were conducted using the NPT ensemble (constant number of molecules, constant pressure and temperature) for a period of 2200 ps including several repeat steps at 298.15 K at four pressures (1000 ps at 1 bar, 100 ps at 100 bar, 100 ps at 10000 bar, and 1000 ps at 1 bar) by adopting the Dreiding force field. [47] The compression/relaxation procedure was applied to the low-density model of the membrane to reach the equilibrium state. High pressure s(100 bar and 10000 bar) were applied only to the compaction part of that compression/relaxation simulation procedure. Next, the final equilibrated structure was used to calculate the membrane properties such as interaction energies and diffusion coefficients at ambient pressure. [48–50] Figure 3 depicts snapshots of the final

equilibrated amorphous cells that MD simulations predicted for the proposed structures. The Crystallographic Information Files (cif) of the equilibrated amorphous cells are provided in the Supporting Information.

The microscopic non-bond interactions can be expressed using the interaction energy, $E_{\text{interaction}}$. Classical MD predicts this energy using: [44,51]

$$E_{\text{int eraction}} = E_{Mixture} - \left(E_{Polyamide} + E_{GQDs}\right) \quad (2)$$

where $E_{\text{interaction}}$, E_{Mixture}, $E_{\text{Polyamide}}$ and E_{GQDs} are the interaction energy, the total energy of the GQDs and the PA mixture, the total energy of the polyamide, and the total energy of GQDs, respectively.

Insights into the mechanism of water transport in each of the proposed structures were obtained from diffusion coefficients calculated from the mean squared displacement (MSD) using: [48]

$$MSD(t) = \frac{1}{N}\sum_{i=1}^{N}\left[r_i(t) - r_i(t_0)\right]^2 \quad (3)$$

where t is the simulation time, N is the number of particles in the system, and $r_i(t_0)$ and $r_i(t)$ are positions of an atom *i* at the initial time (t_0) and at time *t*, respectively. We then determined the diffusion coefficient, *D*, using the Einstein's relation for a three-dimensional system: [48]

$$D = \frac{1}{6}\lim_{t\to\infty}\frac{d(MSD(t))}{dt} \quad (4)$$

The FFV values for the proposed structures (Table 2) were calculated using:

$$FFV_{sim} = \frac{V - V_0}{V} \quad (5)$$

where

$$V_0 = 1.3 \times V_{vdW} \quad (6)$$

V is the volume of the equilibrated simulation cell, V_0 is the occupied volume by polymer, and V_{vdW} is the van der Waals volume of all atoms calculated by the van der Waals surface method. [52]

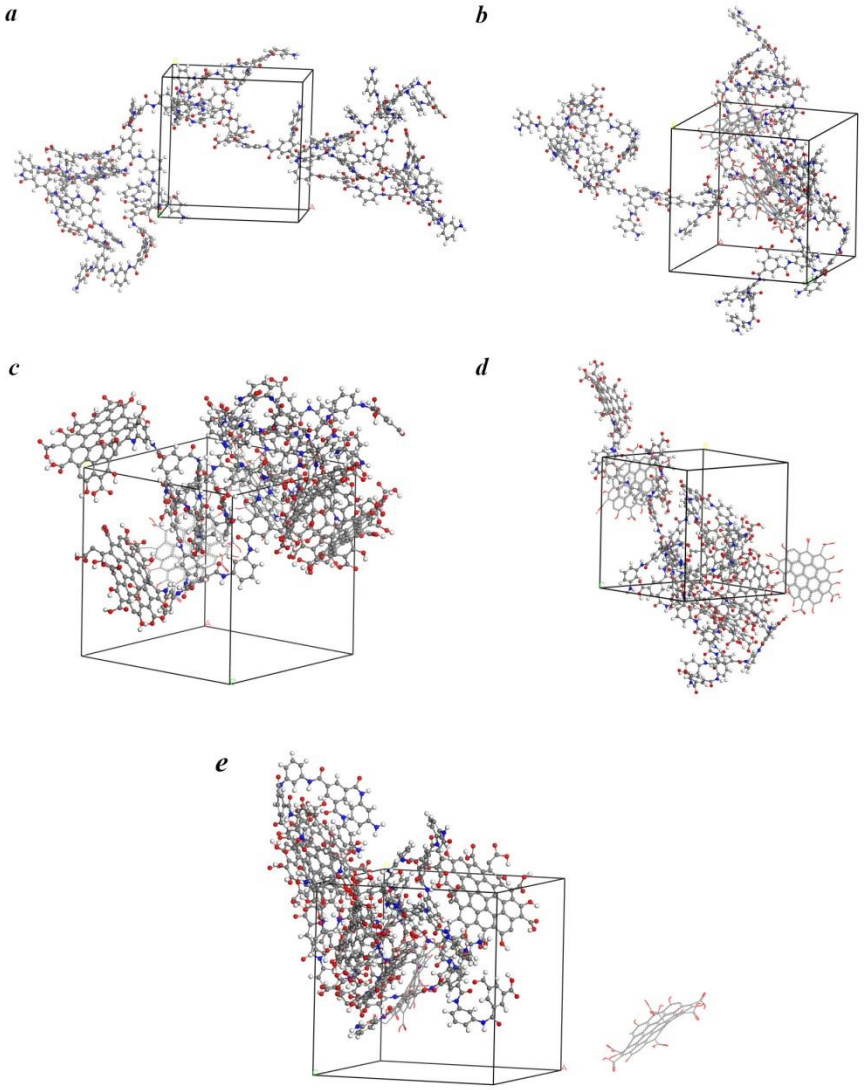

Figure 3: A snapshot of the final equilibrated 3D amorphous cells for (a) P1, (b) P1-GQD, (c) P2-GQD, (d) P3-GQD, and (e) P4-GQD structures.

During the simulations, we considered that the thin film polyamide layer is intrinsically porous. The Monte Carlo algorithm was applied to determine the number of water molecules that should be loaded into each simulation cell. The water diffusion coefficient was calculated after

an equilibrated structure was reached. The maximum water adsorption capacity of each polyamide thin film was determined based on the Grand Canonical Monte Carlo (GCMC) method. [53] In this context, 20 water molecules (a few more than adsorption capacity of each configuration) were loaded into each simulation cell to provide a supper saturated state for the proposed structures during simulations. After loading of the water molecules, a 100-ps NPT simulation was conducted at 298.15 K and 1 bar to reach a new equilibrium and obtain the new density. The water diffusivity of each proposed structure was calculated by the mean square displacement (MSD) analysis (a 5000-ps NVT simulation at 298.15 K). The possibility of intermolecular interactions between GQDs and the PA chains was investigated by calculating the total potential energy of the polymeric mixture in each structure. The energy change difference among different configurations was the basis of the calculations.

3. Results and Discussion

3.1. Molecular interactions of GQDs with a PA chain

A previously-proposed mechanism for the reaction of GQDs with a polyamide chain during the interfacial polymerization between MPD and TMC monomers [41,45] is presented in Figure 2. Based on our observation, during the synthesis of the TFN membranes, after addition of GQDs to the MPD solution a color change from transparent to dark green and finally to black occurred during the first few hours. The color change might be ascribed to reaction of several amine functional groups of the MPD monomers with GQDs forming new covalent bonds during ultra-sonication of the GQDs-MPD suspension. [54] After reaction with MPD or TMC monomers, GQDs can be incorporated to the PA structure. [55,56] In addition, several hydrogen bonds involving the oxygen containing functional groups of GQDs and primary and secondary amines

of the polyamide chains can be formed. Moreover, covalent bonds between GQDs and the carboxyl groups in the linear fraction of the polyamide can be produced through the condensation reaction. This observation is in well agreement with what reported in the literature for a similar scenario. [45] In their study, a color change occurred after the addition of graphene oxide (GO) to the MPD solution. [45] This observation was rationalized as several amine functional groups of the MPD monomers reacted with GO and formed covalent bonds. Furthermore, it has been reported that GO reacts with the acyl chloride groups of TMC to form anhydride and ester linkages. [54] As the MPD aqueous solution is alkalic (pH>7) [57], the dissociation of -OH from carboxyl group of GQDs does not occur, and thus the most probable reaction sites for the functionalization are the aromatic carbon of GQDs, as shown by Liu ae al [58] and Vacchi et al. [59] Moreover, since n-hexane (a non-polar solvent for the TMC solution) cannot deprotonate the carboxyl groups of GQDs, the most probable site for that functionalization is also recognized the aromatic carbon of GQD. Due to the presence of numerous oxygen-containing functional groups, such as hydroxyl and carboxyl groups, on the surface and edges of the GQDs and the existence of amide bonds in the polyamide chain, interactions between the GQDs and PA chains are likely. [55,56] Strong intermolecular interactions and high-density hydrogen bonds should enhance additive-polymer compatibility and reduce structural defects in polymer composites.

MD simulations are applied to determine the interactions between GQDs and the polyamide chains at the molecular level. The predicted energies are presented in Table 1. The more negative is the interaction energy of a structure, the more stable is the structure. Therefore, the more negative total interaction energies of the P1-GQD and P2-GQD suggested the formation of more stable configurations compared to that hypothesized for the P3-GQD and P4-

GQD structures. Although the functionalization with GQDs increases the steric hindrance, the uniform arrangement of GQDs around the functional groups of polyamide chain can lead to enhanced attractive interaction. Furthermore, this higher attractive interaction computed between GQDs and the functional groups of the polyamide chain suggests the formation of hydrogen bonds owing to the presence of donor and acceptor groups in the structure of both GQDs and PA, as depicted in Figure 4. To further verify the presence of hydrogen bonds, radial distances between hydrogen and nitrogen atoms and between hydrogen and oxygen atoms were calculated. In this H-bond detection study, the maximum hydrogen-acceptor distance was set to 2.9 Å, and the minimum donor-hydrogen-acceptor angel to 90°. [60,61] A hydrogen-acceptor distance within 2.7–2.8 Å strongly points to the existence of hydrogen bonds in the structures. [60] The representative snapshot of the final structure obtained from the simulations (Figure 4) shows that the calculated distances between GQDs and the polyamide chain are less than 2.9 Å, which is indicative of electrostatic interactions, based on Jeffrey's categorization. [62]

Table 1: Energies calculated by MD simulations (kcal/mol).

Sample	$E_{Mixture}$	$E_{Polyamide}$	E_{GQDs}	$E_{interaction}$
P1-GQD	1086.98	1063.70	499.56	−476.28
P2-GQD	1415.16	1470.28	381.45	−436.57
P3-GQD	1046.06	1007.68	341.53	−303.15
P4-GQD	1285.76	1292.98	344.12	−351.34

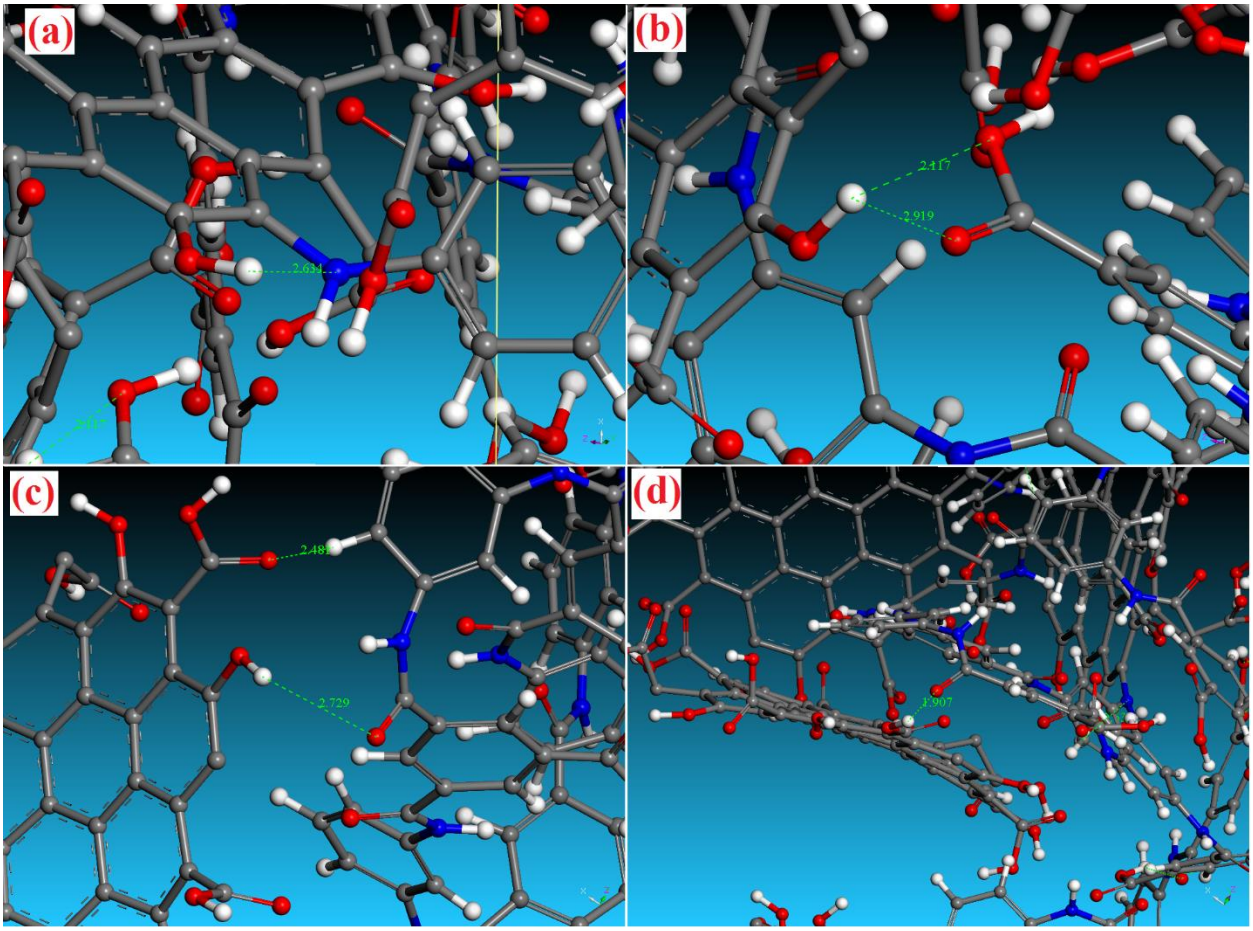

Figure 4: Snapshots obtained at the end of a simulation of P2-GQD, showing the presence of H-bonds between each pair of atoms (red balls = oxygen atoms, grey balls = carbon atoms, blue balls = nitrogen atoms, and white balls = hydrogen atoms).

3.2. Effect of GQDs on the Dynamic Behavior of Water Transport

The predicted interaction energies suggest that the P1-GQD and P2-GQD are the more stable structures among those investigated. To further elucidate the GQD-PA structure, diffusivity coefficients were calculated via MD simulation and compared to the water fluxes obtained from experiments. Figure 5 summarizes the results on the effect of the concentration of GQDs on the experimental water flux of the TFC membranes. [41] The water flux increased with increased GQDs concentration until a medium value and then decreased. The decrease in water flux of the TFN-0.5 was ascribed to GQDs agglomeration and poorer interaction with the

polyamide chains. The enhancement at low concentration may instead also be attributed to improved wettability of the GQDs-PA surfaces compared to those of pristine TFC membrane, facilitating water molecules uptake. [41,44,55] GQDs may also provide extra nano-channels for accelerated transport of water molecules by generating interfacial gaps with the polyamide chains. This phenomenon may concurrently disturb the layer chain packing, which would inevitably increase the free volume of the selective layer and lowers overall selectivity. [41,63,64] Insights into the mechanism of water transport in each of the proposed structures were obtained from diffusion coefficients calculated using the mean squared displacement (MSD). [48]

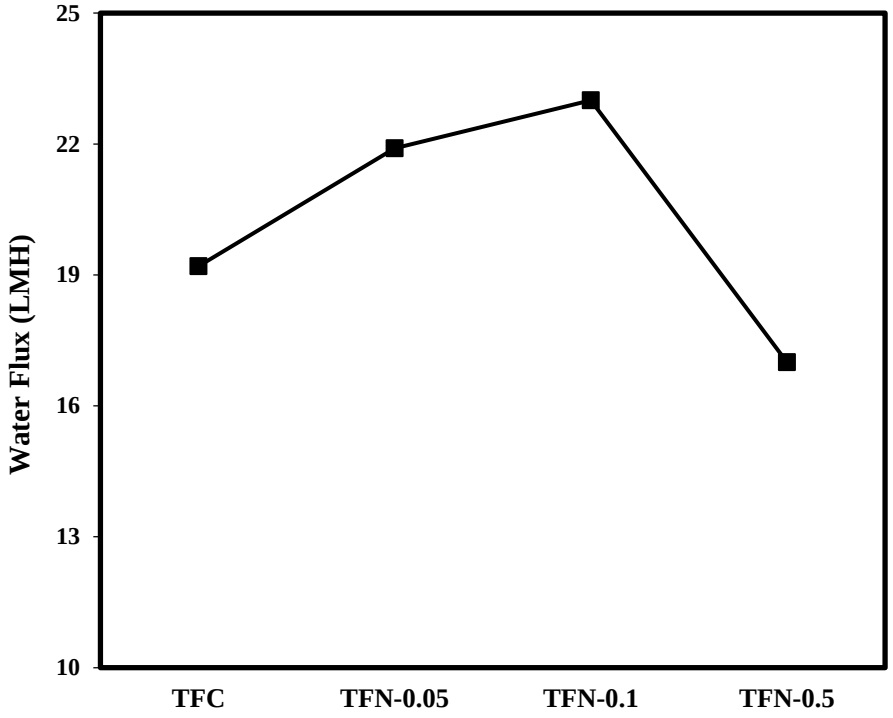

Figure 5: Forward osmosis water flux of the TFC and TFN membranes *vs.* the concentration of GQDs.

Figure 6 reports plots of the MSDs of water molecules at 298.15 K *vs.* time. The MSDs of the P1 and P2-GQD structures increased at much faster rate than those of the P1-GQD, P3-GQD and

P4-GQD, suggesting that the P1 and P2-GQD structures impose a lower resistance to the passage of water molecules.

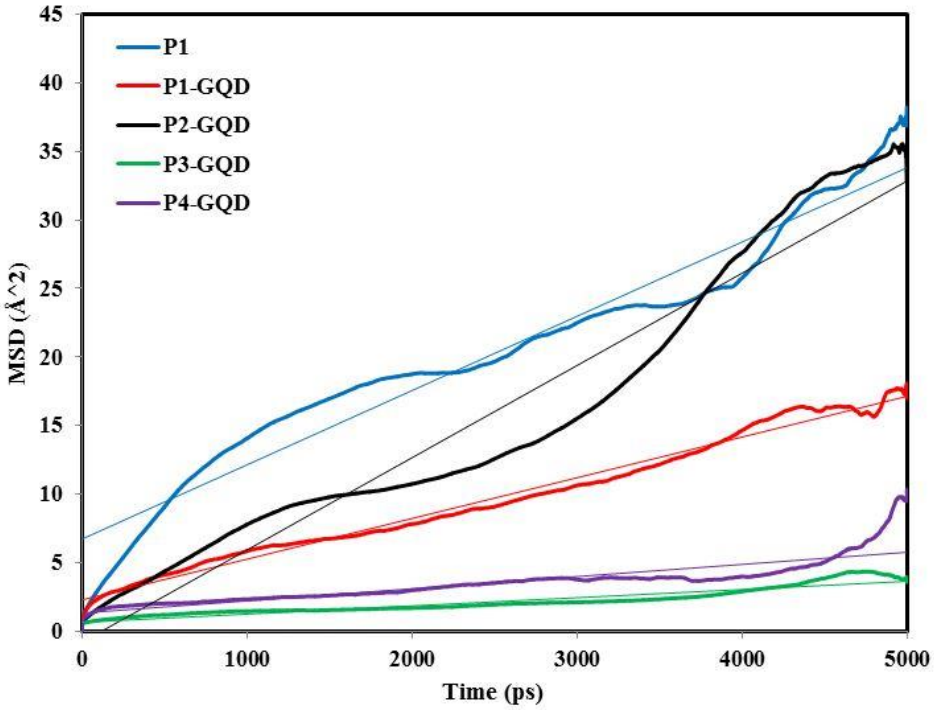

Figure 6: Mean square displacements of water molecules *vs.* NVT simulation time in the four proposed structures at 298.15 K.

Chain movement (depending on the presence of functional groups on polymer chains), density, and fractional free-volume (FFV) are the main physical parameters affecting the diffusion through a membrane. [65] Additionally, the water molecules can be delayed as they are attracted by the hydrophilic terminals (head and tail) inside the narrow channels, a phenomenon that slows down transport. Moreover, the steric hindrance (chain with larger size) and a high-density hydrogen bond distribution also prevent facile transport of water molecules. [44] To better understand the mechanism of water transport, average molecular weights, densities, fractional free volume, and water diffusion coefficients were calculated for the four proposed structures

and presented in Table 2. The first parameter that will be discussed is the diffusion coefficient resulting from the simulations. This parameter follows the following order: P2-GQD> P1> P1-GQD > P4-GQD > P3-GQD, consistent with the results presented in Figure 6. Also based on the other parameters presented in Table 2 and discussed below, we actually hypothesize that the higher diffusion coefficients of the P2-GQD structure may be explained by the lower density of hydrogen bonds, [65] lower transport resistance, [66] and lower affinity to water molecules inside the narrow channels. [67,68] The enhanced diffusivity coefficient of the P2-GQD structure also agrees well with increased water fluxes obtained from experiments and the low diffusion coefficient computed for P4-GQD structure also confirms the experimental observations suggesting that this configuration is unlikely. The results of interaction energies supported by the computed layer properties and water transport parameters imply that the P2-GQD structure is the most likely structure of the TFN membranes. The strong interaction mechanism of the GQDs with MPD monomers and the weak interaction mechanism of the GQDs with a polyamide chain occurring in this structure are shown in Figure 7. To summarize, the higher water diffusivity of P2-GQD compared to the pristine TFC may be attributed to a larger surface wettability and an overall lower resistance against the passage of water molecules.

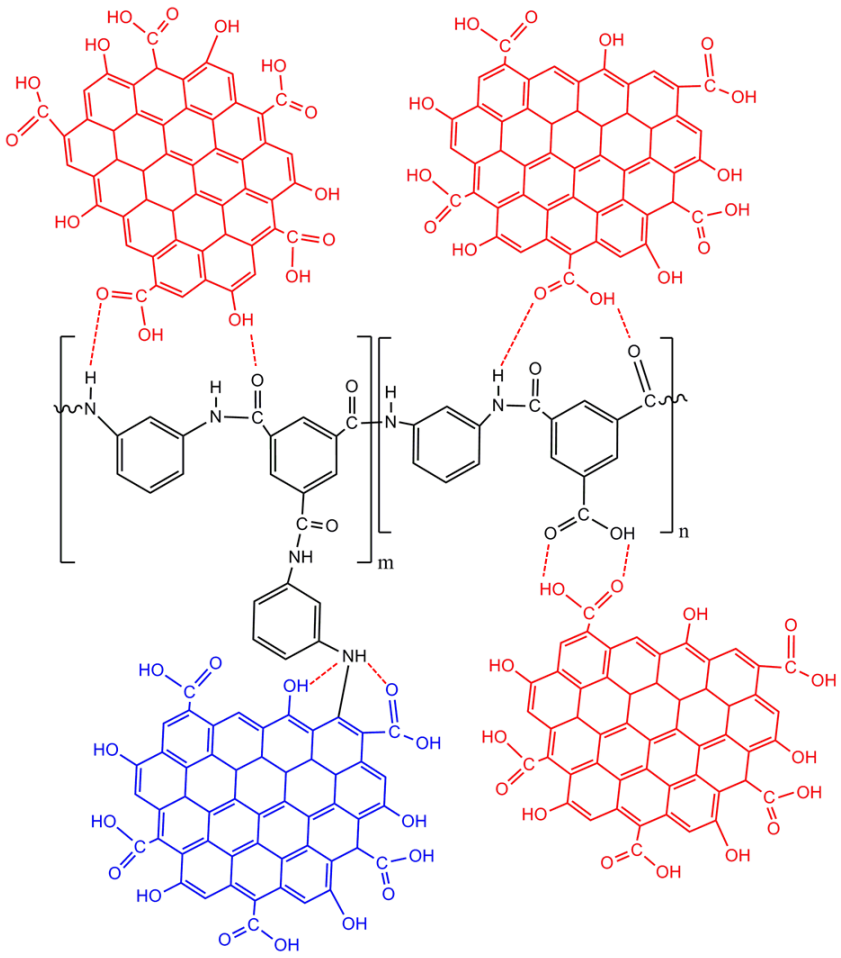

Figure 7: The mechanism for the interactions of the GQDs with MPD and TMC units, proposed based on the MD simulations conducted in this study.

To complete the picture of the water transport mechanism across the nanocomposite layer, the other parameters calculated by the MD simulations are presented in Table 2. The computed density of the pristine polyamide structure is about 1.186 g/cm^3, which is consistent with the reported values of 1.2 and 1.24 g/cm^3; [26,69] see Table 2. The density of P1-GQD is not significantly different from this value, while P2-GQD, P3-GQD and P4-GQD densities surprisingly increased to 1.38 g/cm^3 and 1.35 g/cm^3 with the incorporation of GQDs. Figure 8 shows the simulated morphology of the fractional free volume and its distribution in the proposed structures. The FFV values for the proposed structures were listed in Table 2. The

363 fractional accessible volume (FAV) was also calculated based on the diameter of water molecule
364 (2.75 Å) and according to the solvent excluded surface (Connolly surface) method, [70] while
365 ignoring the factor of 1.3 (Table 2).

366 Despite the seemingly reasonable hypothesis that GQDs provide extra nano-channels and
367 generate more free volume, the incorporation of GQDs into to the amorphous cell seems to
368 decrease the FFV, due to the overall increased density of the structure and owing to a good
369 interaction with the polymer chains, thus creating a seamless interface. More connected voids
370 would provide more water diffusion paths, while smaller and isolated voids in the GQDs-
371 functionalized polyamide structure are associated with a lower density of effective channels for
372 water molecules passage. [71] However, as discussed earlier the P2-GQD structure was associated
373 with higher water diffusion despite its increased density and reduced FFV. As such, the density
374 and FFV of the selective layer do not seem to be the main factors affecting the overall water
375 transport characteristics of the membrane. In this case, the presence of shorter paths for transport
376 of water molecules in the P2-GQD structure may instead be considered as the main features
377 allowing faster water passage despite higher overall density of the selective layer. [72]

378 **Table 2:** Predicted average molecular weights of polymer chains, densities of composites, and diffusivity
379 coefficients of water in the polymeric thin films.

Sample	Molecular Weight (g/mol)	Predicted Density (cm^3/g)	$D \times 10^8$ (cm^2/s)	FFV (–)	FAV (–)
P1	10476.2	1.19	9.00	0.233	0.172
P1-GQD	10476.2	1.19	5.00	0.253	0.219
P2-GQD	10820.9	1.38	11.17	0.175	0.141
P3-GQD	9766.3	1.38	1.00	0.171	0.127
P4-GQD	10741.0	1.35	1.50	0.193	0.165

380

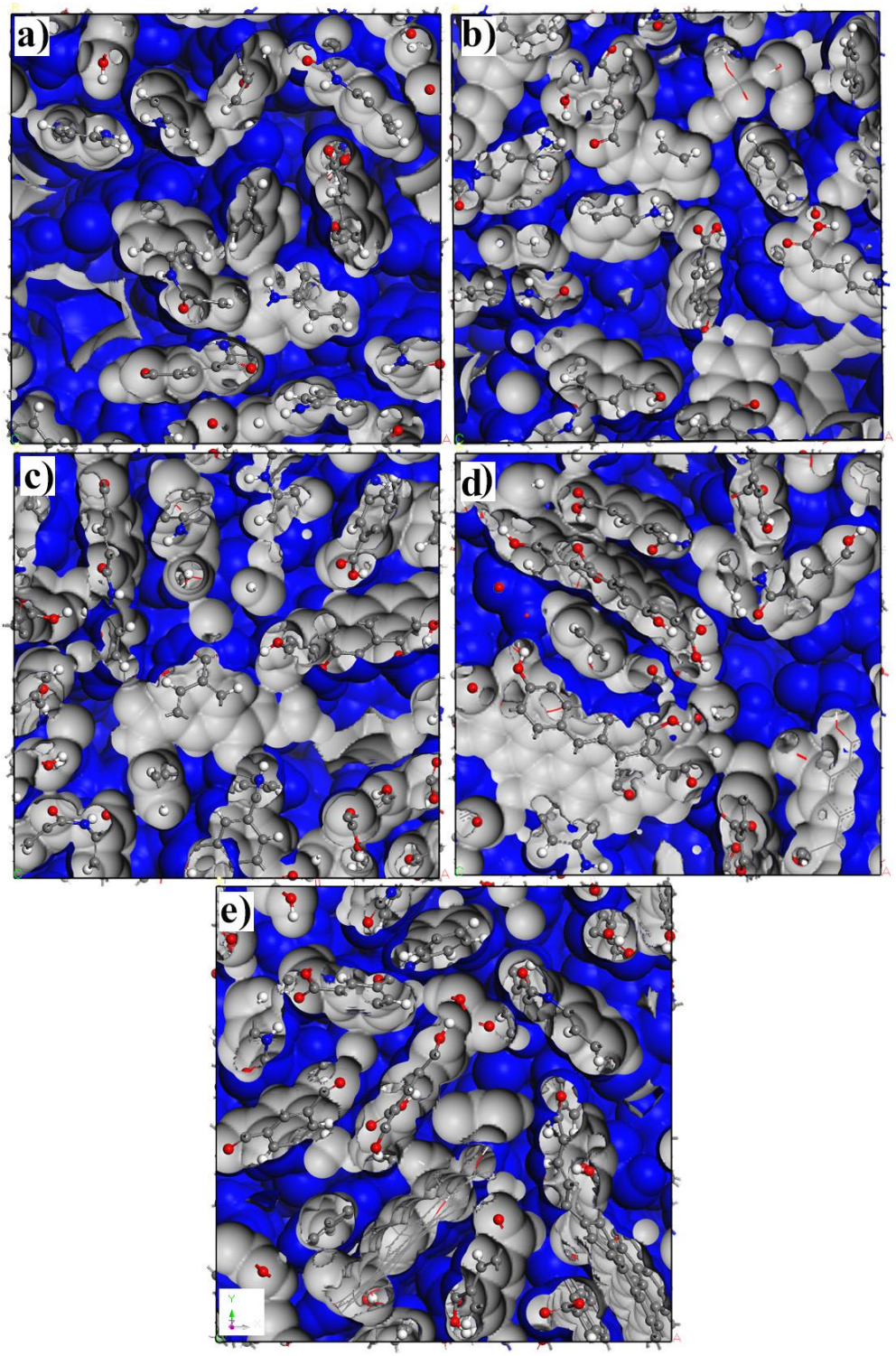

Figure 8. Morphology of the free volume in (a) P1, (b) P1-GQD, (c) P2-GQD, (d) P3-GQD, and (e) P4-GQD structures (blue areas = free volume).

4. Conclusion

Several chemical structure models of the polyamide membranes incorporating graphene quantum dots (GDQs) were proposed. Using molecular dynamics (MD), the interaction energies, densities, water diffusion coefficients, mean square displacements, and FFVs were predicted for each of the structures. Experimental data and MD predictions indicated that the chemical structure in which the GQDs form covalent bonds with the amine-containing monomers and which forms hydrogen bonds with the polyamide (PA) chains is the most likely structure for the nanocomposite GQD-PA membrane. The considerably higher water diffusion in such a structure compared to the other hypothesize configurations and to the pristine polyamide was found to be due to a larger surface wettability (because of the presence of GQDs) combined with a lower chance of linkages formed while water molecules move through the layer. This phenomenon seems to overpower the effect provided by a relatively high density and low FFV of the resulting structure. Another critical characteristic allowing an unimpaired nanocomposite selective layer is the high PA-GQDs compatibility, preventing the formation of large interfacial voids that would decrease selectivity and in turn reduce the water transport in forward osmosis. In summary, our simulations suggest that a high-performance nanocomposite layer is one where a relatively low number of fillers interact strongly with the polymer chains to form a seamless structure that maintains selectivity and that, while increasing water uptake by adsorption at the membrane-solution interface, does not hold back water molecules as it reduces the likelihood of water-layer hydrogen bonding. The hierarchical simulation protocol applied in this study may be extended to explore other nanocomposite membranes, and to gain an improved molecular-level understanding with the goal to develop high-performance membranes for a wide range of applications.

Supporting information

Crystallographic Information File (CIF) of the equilibrated structure of each simulation cell and the 3D atomic models of GQD and the monomers in the ".mol" format.

Acknowledgment

The authors acknowledge Babol Noshirvani University of Technology for financially support of this project (BNUT/925150005/94 and BNUT/ 4-6130593/97). The authors are also grateful for the research collaboration between Babol Noshirvani University of Technology with Politecnico di Torino and Drexel University.

References

(1) Li, D.; Wang, H. Recent Developments in Reverse Osmosis Desalination Membranes. *J. Mater. Chem.* **2010**, *20*, 4551.

(2) Song, Y.; Xu, F.; Wei, M.; Wang, Y. Water Flow inside Polamide Reverse Osmosis Membranes: A Non-Equilibrium Molecular Dynamics Study. *J. Phys. Chem. B* **2017**, *121* (7), 1715–1722. https://doi.org/10.1021/acs.jpcb.6b11536.

(3) Firouzjaei, M. D.; Seyedpour, S. F.; Aktij, S. A.; Giagnorio, M.; Bazrafshan, N.; Mollahosseini, A.; Samadi, F.; Ahmadalipour, S.; Firouzjaei, F. D.; Esfahani, M. R. Recent Advances in Functionalized Polymer Membranes for Biofouling Control and Mitigation in Forward Osmosis. *J. Memb. Sci.* **2019**, 117604.

(4) Zirehpour, A.; Rahimpour, A.; Khoshhal, S.; Firouzjaei, M. D.; Ghoreyshi, A. A. The Impact of MOF Feasibility to Improve the Desalination Performance and Antifouling Properties of FO Membranes. *RSC Adv.* **2016**, *6* (74), 70174–70185.

(5) Esfahani, M. R.; Aktij, S. A.; Dabaghian, Z.; Firouzjaei, M. D.; Rahimpour, A.; Eke, J.; Escobar, I. C.; Abolhassani, M.; Greenlee, L. F.; Esfahani, A. R. Nanocomposite Membranes for Water Separation and Purification: Fabrication, Modification, and Applications. *Sep. Purif. Technol.* **2018**.

(6) Chan, W.-F.; Marand, E.; Martin, S. M. Novel Zwitterion Functionalized Carbon Nanotube Nanocomposite Membranes for Improved RO Performance and Surface Anti-Biofouling Resistance. *J. Memb. Sci.* **2016**, *509*, 125–137. https://doi.org/https://doi.org/10.1016/j.memsci.2016.02.014.

(7) Kim, H. J.; Choi, K.; Baek, Y.; Kim, D. G.; Shim, J.; Yoon, J.; Lee, J. C. High-Performance Reverse Osmosis CNT/Polyamide Nanocomposite Membrane by Controlled Interfacial Interactions. *ACS Appl. Mater. Interfaces* **2014**, *6* (4), 2819.

(8) Seyedpour, S. F.; Rahimpour, A.; Najafpour, G. Facile In-Situ Assembly of Silver-Based MOFs to Surface Functionalization of TFC Membrane: A Novel Approach toward Long-Lasting Biofouling Mitigation. *J. Memb. Sci.* **2019**, *573*, 257–269. https://doi.org/https://doi.org/10.1016/j.memsci.2018.12.016.

(9) Zirehpour, A.; Rahimpour, A.; Arabi Shamsabadi, A.; Sharifian Gh., M.; Soroush, M. Mitigation of Thin-Film Composite Membrane Biofouling via Immobilizing Nano-Sized Biocidal Reservoirs in the Membrane Active Layer. *Environ. Sci. Technol.* **2017**, *51*, 5511.

(10) Firouzjaei, M. D.; Shamsabadi, A. A.; Aktij, S. A.; Seyedpour, S. F.; Sharifian Gh., M.; Rahimpour, A.; Esfahani, M. R.; Ulbricht, M.; Soroush, M. Exploiting Synergetic Effects of Graphene Oxide and a Silver-Based Metal–Organic Framework To Enhance Antifouling and Anti-Biofouling Properties of Thin-Film Nanocomposite Membranes.

ACS Appl. Mater. Interfaces **2018**, *10* (49), 42967–42978. https://doi.org/10.1021/acsami.8b12714.

(11) Prakash Rao, A.; Joshi, S. V; Trivedi, J. J.; Devmurari, C. V; Shah, V. J. Structure–Performance Correlation of Polyamide Thin Film Composite Membranes: Effect of Coating Conditions on Film Formation. *J. Memb. Sci.* **2003**, *211* (1), 13–24. https://doi.org/https://doi.org/10.1016/S0376-7388(02)00305-8.

(12) Huang, Y.-H.; Chao, W.-C.; Hung, W.-S.; An, Q.-F.; Chang, K.-S.; Huang, S.-H.; Tung, K.-L.; Lee, K.-R.; Lai, J.-Y. Investigation of Fine-Structure of Polyamide Thin-Film Composite Membrane under Swelling Effect by Positron Annihilation Lifetime Spectroscopy and Molecular Dynamics Simulation. *J. Memb. Sci.* **2012**, *417–418*, 201–209. https://doi.org/https://doi.org/10.1016/j.memsci.2012.06.036.

(13) Košutić, K.; Kunst, B. RO and NF Membrane Fouling and Cleaning and Pore Size Distribution Variations. *Desalination* **2002**, *150* (2), 113–120. https://doi.org/https://doi.org/10.1016/S0011-9164(02)00936-0.

(14) Szymczyk, A.; Fievet, P. Investigating Transport Properties of Nanofiltration Membranes by Means of a Steric, Electric and Dielectric Exclusion Model. *J. Memb. Sci.* **2005**, *252* (1), 77–88. https://doi.org/https://doi.org/10.1016/j.memsci.2004.12.002.

(15) Zhang, N.; Chen, S.; Yang, B.; Huo, J.; Zhang, X.; Bao, J.; Ruan, X.; He, G. Effect of Hydrogen-Bonding Interaction on the Arrangement and Dynamics of Water Confined in a Polyamide Membrane: A Molecular Dynamics Simulation. *J. Phys. Chem. B* **2018**, *122* (17), 4719–4728. https://doi.org/10.1021/acs.jpcb.7b12790.

(16) Gai, J.-G.; Gong, X.-L.; Kang, W.-L.; Zhang, X.; Wang, W.-W. Key Factors Influencing Water Diffusion in Aromatic PA Membrane: Hydrates, Nanochannels and Functional

Groups. *Desalination* **2014**, *333* (1), 52–58. https://doi.org/https://doi.org/10.1016/j.desal.2013.11.028.

(17) Arabi Shamsabadi, A.; Sharifian Gh, M.; Anasori, B.; Soroush, M. Antimicrobial Mode-of-Action of Colloidal Ti3C2T x MXene Nanosheets. *ACS Sustain. Chem. Eng.* **2018**, *6* (12), 16586–16596.

(18) Najafi, M.; Sadeghi, M.; Shamsabadi, A. A.; Dinari, M.; Soroush, M. Polysulfone Membranes Incorporated with Reduced Graphene Oxide Nanoparticles for Enhanced Olefin/Paraffin Separation. *ChemistrySelect* **2020**, *5* (12), 3675–3681.

(19) Li, J.; Yin, L.; Qiu, G.; Li, X.; Liu, Q.; Xie, J. A Photo-Bactericidal Thin Film Composite Membrane for Forward Osmosis. *J. Mater. Chem. A* **2015**, *3* (13), 6781–6786. https://doi.org/10.1039/C5TA00430F.

(20) Lin, L.; Rong, M.; Luo, F.; Chen, D.; Wang, Y.; Chen, X. Luminescent Graphene Quantum Dots as New Fluorescent Materials for Environmental and Biological Applications. *TrAC Trends Anal. Chem.* **2014**, *54*, 83–102. https://doi.org/https://doi.org/10.1016/j.trac.2013.11.001.

(21) Firouzjaei, M. D.; Shamsabadi, A. A.; Gh, M. S.; Rahimpour, A.; Soroush, M. A Novel Nanocomposite with Superior Antibacterial Activity: A Silver-Based Metal Organic Framework Embellished with Graphene Oxide. *Adv. Mater. Interfaces* **2018**.

(22) Luo, P.; Ji, Z.; Li, C.; Shi, G. Aryl-Modified Graphene Quantum Dots with Enhanced Photoluminescence and Improved PH Tolerance. *Nanoscale* **2013**, *5* (16), 7361–7367. https://doi.org/10.1039/C3NR02156D.

(23) Tetsuka, H.; Asahi, R.; Nagoya, A.; Okamoto, K.; Tajima, I.; Ohta, R.; Okamoto, A. Optically Tunable Amino-Functionalized Graphene Quantum Dots. *Adv. Mater.* **2012**, *24*

(39), 5333–5338. https://doi.org/10.1002/adma.201201930.

(24) Firouzjaei, M. D.; Afkhami, F. A.; Esfahani, M. R.; Turner, C. H.; Nejati, S. Experimental and Molecular Dynamics Study on Dye Removal from Water by a Graphene Oxide-Copper-Metal Organic Framework Nanocomposite. *J. Water Process Eng.* **2020**, *34*, 101180.

(25) Wei, T.; Zhang, L.; Zhao, H.; Ma, H.; Sajib, M. S. J.; Jiang, H.; Murad, S. Aromatic Polyamide Reverse-Osmosis Membrane: An Atomistic Molecular Dynamics Simulation. *J. Phys. Chem. B* **2016**, *120*, 10311.

(26) Kolev, V.; Freger, V. Hydration, Porosity and Water Dynamics in the Polyamide Layer of Reverse Osmosis Membranes: A Molecular Dynamics Study. *Polymer (Guildf).* **2014**, *55* (6), 1420–1426. https://doi.org/https://doi.org/10.1016/j.polymer.2013.12.045.

(27) Arabi Shamsabadi, A.; Pournaghshband Isfahani, A.; Khoshhal Salestan, S.; Rahimpour, A.; Ghalei, B.; Sivaniah, E.; Soroush, M. Pushing Rubbery Polymer Membranes to Be Economic for CO2 Separation: Embedment with Ti3C2Tx MXene Nanosheets. *ACS Appl. Mater. Interfaces* **2019**. https://doi.org/10.1021/acsami.9b19960.

(28) Lu, J.; Liu, D.; Yang, X.; Zhao, Y.; Liu, H.; Tang, H.; Cui, F. Molecular Dynamics Simulations of Interfacial Interactions between Small Nanoparticles during Diffusion-Limited Aggregation. *Appl. Surf. Sci.* **2015**, *357*, 1114–1121. https://doi.org/https://doi.org/10.1016/j.apsusc.2015.09.142.

(29) Pogrebnjak, A. D.; Bondar, O. V; Abadias, G.; Ivashchenko, V.; Sobol, O. V; Jurga, S.; Coy, E. Structural and Mechanical Properties of NbN and Nb-Si-N Films: Experiment and Molecular Dynamics Simulations. *Ceram. Int.* **2016**, *42* (10), 11743–11756. https://doi.org/https://doi.org/10.1016/j.ceramint.2016.04.095.

(30) Goudeau, S.; Charlot, M.; Vergelati, C.; Müller-Plathe, F. Atomistic Simulation of the Water Influence on the Local Structure of Polyamide 6,6. *Macromolecules* **2004**, *37*, 8072.

(31) Kao, S.-T.; Huang, Y.-H.; Liao, K.-S.; Hung, W.-S.; Chang, K.-S.; De Guzman, M.; Huang, S.-H.; Wang, D.-M.; Tung, K.-L.; Lee, K.-R.; et al. Applications of Positron Annihilation Spectroscopy and Molecular Dynamics Simulation to Aromatic Polyamide Pervaporation Membranes. *J. Memb. Sci.* **2010**, *348* (1), 117–123. https://doi.org/https://doi.org/10.1016/j.memsci.2009.10.048.

(32) Gao, W.; She, F.; Zhang, J.; Dumée, L. F.; He, L.; Hodgson, P. D.; Kong, L. Understanding Water and Ion Transport Behaviour and Permeability through Poly(Amide) Thin Film Composite Membrane. *J. Memb. Sci.* **2015**, *487*, 32–39. https://doi.org/https://doi.org/10.1016/j.memsci.2015.03.052.

(33) Shen, M.; Keten, S.; Lueptow, R. M. Dynamics of Water and Solute Transport in Polymeric Reverse Osmosis Membranes via Molecular Dynamics Simulations. *J. Memb. Sci.* **2016**, *506*, 95–108. https://doi.org/https://doi.org/10.1016/j.memsci.2016.01.051.

(34) Lebrón-Colón, M.; Meador, M. A.; Gaier, J. R.; Solá, F.; Scheiman, D. A.; McCorkle, L. S. Reinforced Thermoplastic Polyimide with Dispersed Functionalized Single Wall Carbon Nanotubes. *ACS Appl. Mater. Interfaces* **2010**, *2* (3), 669–676. https://doi.org/10.1021/am900682s.

(35) Chan, W. F.; Chen, H. Y.; Surapathi, A.; Taylor, M. G.; Hao, X. H.; Marand, E.; Johnson, J. K. Zwitterion Functionalized Carbon Nanotube/Polyamide Nanocomposite Membranes for Water Desalination. *ACS Nano* **2013**, *7* (6), 5308.

(36) Inukai, S.; Cruz-Silva, R.; Ortiz-Medina, J.; Morelos-Gomez, A.; Takeuchi, K.; Hayashi,

T.; Tanioka, A.; Araki, T.; Tejima, S.; Noguchi, T.; et al. High-Performance Multi-Functional Reverse Osmosis Membranes Obtained by Carbon Nanotube·polyamide Nanocomposite. *Sci. Rep.* **2015**, *5*, 13562.

(37) Araki, T.; Cruz-Silva, R.; Tejima, S.; Takeuchi, K.; Hayashi, T.; Inukai, S.; Noguchi, T.; Tanioka, A.; Kawaguchi, T.; Terrones, M.; et al. Molecular Dynamics Study of Carbon Nanotubes/Polyamide Reverse Osmosis Membranes: Polymerization, Structure, and Hydration. *ACS Appl. Mater. Interfaces* **2015**, *7* (44), 24566–24575. https://doi.org/10.1021/acsami.5b06248.

(38) Eslami, H.; Behrouz, M. Molecular Dynamics Simulation of a Polyamide-66/Carbon Nanotube Nanocomposite. *J. Phys. Chem. C* **2014**, *118* (18), 9841–9851. https://doi.org/10.1021/jp501672t.

(39) Aztatzi-Pluma, D.; Castrejón-González, E. O.; Almendarez-Camarillo, A.; Alvarado, J. F. J.; Durán-Morales, Y. Study of the Molecular Interactions between Functionalized Carbon Nanotubes and Chitosan. *J. Phys. Chem. C* **2016**, *120* (4), 2371–2378. https://doi.org/10.1021/acs.jpcc.5b08136.

(40) Rahimpour, A.; Jahanshahi, M.; Khalili, S.; Mollahosseini, A.; Zirepour, A.; Rajaeian, B. Novel Functionalized Carbon Nanotubes for Improving the Surface Properties and Performance of Polyethersulfone (PES) Membrane. *Desalination* **2012**, *286* (Supplement C), 99–107. https://doi.org/https://doi.org/10.1016/j.desal.2011.10.039.

(41) Seyedpour, S. F.; Rahimpour, A.; Shamsabadi, A. A.; Soroush, M. Improved Performance and Antifouling Properties of Thin-Film Composite Polyamide Membranes Modified with Nano-Sized Bactericidal Graphene Quantum Dots for Forward Osmosis. *Chem. Eng. Res. Des.* **2018**, *139*, 321–334. https://doi.org/https://doi.org/10.1016/j.cherd.2018.09.041.

(42) Dong, Y.; Shao, J.; Chen, C.; Li, H.; Wang, R.; Chi, Y.; Lin, X.; Chen, G. Blue Luminescent Graphene Quantum Dots and Graphene Oxide Prepared by Tuning the Carbonization Degree of Citric Acid. *Carbon N. Y.* **2012**, *50* (12), 4738–4743. https://doi.org/https://doi.org/10.1016/j.carbon.2012.06.002.

(43) He, Y.; Wang, X.; Sun, J.; Jiao, S.; Chen, H.; Gao, F.; Wang, L. Fluorescent Blood Glucose Monitor by Hemin-Functionalized Graphene Quantum Dots Based Sensing System. *Anal. Chim. Acta* **2014**, *810*, 71–78. https://doi.org/https://doi.org/10.1016/j.aca.2013.11.059.

(44) Rahimpour, A.; Seyedpour, S. F.; Aghapour Aktij, S.; Dadashi Firouzjaei, M.; Zirehpour, A.; Arabi Shamsabadi, A.; Khoshhal Salestan, S.; Jabbari, M.; Soroush, M. Simultaneous Improvement of Antimicrobial, Antifouling, and Transport Properties of Forward Osmosis Membranes with Immobilized Highly-Compatible Polyrhodanine Nanoparticles. *Environ. Sci. Technol.* **2018**, *52* (9), 5246–5258. https://doi.org/10.1021/acs.est.8b00804.

(45) Ali, M. E. A.; Wang, L.; Wang, X.; Feng, X. Thin Film Composite Membranes Embedded with Graphene Oxide for Water Desalination. *Desalination* **2016**, *386*, 67–76. https://doi.org/https://doi.org/10.1016/j.desal.2016.02.034.

(46) Xu, S.; Li, F.; Su, B.; Hu, M. Z.; Gao, X.; Gao, C. Novel Graphene Quantum Dots (GQDs)-Incorporated Thin Film Composite (TFC) Membranes for Forward Osmosis (FO) Desalination. *Desalination* **2019**, *451*, 219–230. https://doi.org/https://doi.org/10.1016/j.desal.2018.04.004.

(47) Mayo, S. L.; Olafson, B. D.; Goddard, W. A. DREIDING - A Generic Force-Field for Molecular Simulations. *J. Phys. Chem.* **1990**, *94* (26), 8897.

(48) Kebria, M. R. S.; Rahimpour, A.; Bakeri, G.; Abedini, R. Experimental and Theoretical

Investigation of Thin ZIF-8/Chitosan Coated Layer on Air Gap Membrane Distillation Performance of PVDF Membrane. *Desalination* **2019**, *450*, 21–32. https://doi.org/https://doi.org/10.1016/j.desal.2018.10.023.

(49) Chen, Y.-R.; Chen, L.-H.; Chang, K.-S.; Chen, T.-H.; Lin, Y.-F.; Tung, K.-L. Structural Characteristics and Transport Behavior of Triptycene-Based PIMs Membranes: A Combination Study Using Ab Initio Calculation and Molecular Simulations. *J. Memb. Sci.* **2016**, *514*, 114–124. https://doi.org/https://doi.org/10.1016/j.memsci.2016.04.063.

(50) Du, N.; Park, H. B.; Robertson, G. P.; Dal-Cin, M. M.; Visser, T.; Scoles, L.; Guiver, M. D. Polymer Nanosieve Membranes for CO2-Capture Applications. *Nat. Mater.* **2011**, *10* (5), 372–375. https://doi.org/10.1038/nmat2989.

(51) Mozafari, M.; Seyedpour, S. F.; Salestan, S. K.; Rahimpour, A.; Shamsabadi, A. A.; Firouzjaei, M. D.; Esfahani, M. R.; Tiraferri, A.; Mohsenian, H.; Sangermano, M.; et al. Facile Cu-BTC Surface Modification of Thin Chitosan Film Coated Polyethersulfone Membranes with Improved Antifouling Properties for Sustainable Removal of Manganese. *J. Memb. Sci.* **2019**, *588*, 117200. https://doi.org/https://doi.org/10.1016/j.memsci.2019.117200.

(52) Bondi, A. Van Der Waals Volumes and Radii. *J. Phys. Chem.* **1964**, *68* (3), 441–451. https://doi.org/10.1021/j100785a001.

(53) Salestan, S. K.; Taghizadeh, M. The Effect of Impurity on the Separation of CO2 from N2 by MCM-41: A Simulation Study. *Chem. Phys.* **2019**, *524*, 124–130. https://doi.org/https://doi.org/10.1016/j.chemphys.2019.05.014.

(54) Shen, L.; Xiong, S.; Wang, Y. Graphene Oxide Incorporated Thin-Film Composite Membranes for Forward Osmosis Applications. *Chem. Eng. Sci.* **2016**, *143*, 194–205.

https://doi.org/https://doi.org/10.1016/j.ces.2015.12.029.

(55) Bano, S.; Mahmood, A.; Kim, S.-J.; Lee, K.-H. Graphene Oxide Modified Polyamide Nanofiltration Membrane with Improved Flux and Antifouling Properties. *J. Mater. Chem. A* **2015**, *3* (5), 2065–2071. https://doi.org/10.1039/C4TA03607G.

(56) Saha, N. K.; Joshi, S. V. Performance Evaluation of Thin Film Composite Polyamide Nanofiltration Membrane with Variation in Monomer Type. *J. Memb. Sci.* **2009**, *342* (1), 60–69. https://doi.org/https://doi.org/10.1016/j.memsci.2009.06.025.

(57) Peng, L. E.; Yao, Z.; Liu, X.; Deng, B.; Guo, H.; Tang, C. Y. Tailoring Polyamide Rejection Layer with Aqueous Carbonate Chemistry for Enhanced Membrane Separation: Mechanistic Insights, Chemistry-Structure-Property Relationship, and Environmental Implications. *Environ. Sci. Technol.* **2019**, *53* (16), 9764–9770. https://doi.org/10.1021/acs.est.9b03210.

(58) Liu, S.; Yu, B.; Zhang, T. Preparation of Crumpled Reduced Graphene Oxide–Poly(p-Phenylenediamine) Hybrids for the Detection of Dopamine. *J. Mater. Chem. A* **2013**, *1* (42), 13314–13320. https://doi.org/10.1039/C3TA12594G.

(59) Vacchi, I. A.; Spinato, C.; Raya, J.; Bianco, A.; Ménard-Moyon, C. Chemical Reactivity of Graphene Oxide towards Amines Elucidated by Solid-State NMR. *Nanoscale* **2016**, *8* (28), 13714–13721. https://doi.org/10.1039/C6NR03846H.

(60) Tang, C.; Li, X.; Li, Z.; Hao, J. Interfacial Hydrogen Bonds and Their Influence Mechanism on Increasing the Thermal Stability of Nano-SiO2-Modified Meta-Aramid Fibres. *Polymers* . 2017. https://doi.org/10.3390/polym9100504.

(61) Callam, C. S.; Singer, S. J.; Lowary, T. L.; Hadad, C. M. Computational Analysis of the Potential Energy Surfaces of Glycerol in the Gas and Aqueous Phases: Effects of Level of

Theory, Basis Set, and Solvation on Strongly Intramolecularly Hydrogen-Bonded Systems. *J. Am. Chem. Soc.* **2001**, *123* (47), 11743–11754. https://doi.org/10.1021/ja011785r.

(62) Jeffrey, G. A. J.; Jeffrey, G. A. *An Introduction to Hydrogen Bonding*; Topics in Physical Chemistry - Oxford University Press; Oxford University Press, 1997.

(63) Song, X.; Zhou, Q.; Zhang, T.; Xu, H.; Wang, Z. Pressure-Assisted Preparation of Graphene Oxide Quantum Dot-Incorporated Reverse Osmosis Membranes: Antifouling and Chlorine Resistance Potentials. *J. Mater. Chem. A* **2016**, *4* (43), 16896–16905. https://doi.org/10.1039/C6TA06636D.

(64) Wu, H.; Tang, B.; Wu, P. Optimizing Polyamide Thin Film Composite Membrane Covalently Bonded with Modified Mesoporous Silica Nanoparticles. *J. Memb. Sci.* **2013**, *428*, 341–348. https://doi.org/https://doi.org/10.1016/j.memsci.2012.10.053.

(65) Bai, R.; Wang, H.; Zhang, P.; Xiao, B.; Jiang, B.; Zhou, G. Molecular Dynamics Simulation of the Diffusion Behavior of Water in Poly(Vinylidene Fluoride)/Silica Hybrid Membranes. *RSC Adv.* **2015**, *5* (70), 57147–57154. https://doi.org/10.1039/C5RA09261B.

(66) Chang, K.-S.; Wang, Y.-L.; Kang, C.-H.; Wei, H.-J.; Weng, Y.-H.; Tung, K.-L. Molecular Dynamics Simulations of Polymeric Structure and Alcohol-Membrane Surface Affinity of Aromatic Polyamide Membranes. *J. Memb. Sci.* **2011**, *382* (1), 30–40. https://doi.org/https://doi.org/10.1016/j.memsci.2011.07.043.

(67) Wu, H.-C.; Yoshioka, T.; Nagasawa, H.; Kanezashi, M.; Tsuru, T.; Saeki, D.; Matsuyama, H. Preparation of Cyclic Peptide Nanotube Structures and Molecular Simulation of Water Adsorption and Diffusion. *J. Memb. Sci.* **2017**, *537*, 101–110. https://doi.org/https://doi.org/10.1016/j.memsci.2017.04.060.

(68) Wu, H.-C.; Yoshioka, T.; Nakagawa, K.; Shintani, T.; Tsuru, T.; Saeki, D.; Shaikh, A. R.; Matsuyama, H. Preparation of Amphotericin B-Ergosterol Structures and Molecular Simulation of Water Adsorption and Diffusion. *J. Memb. Sci.* **2018**, *545*, 229–239. https://doi.org/https://doi.org/10.1016/j.memsci.2017.09.032.

(69) Zhang, X.; Cahill, D. G.; Coronell, O.; Mariñas, B. J. Absorption of Water in the Active Layer of Reverse Osmosis Membranes. *J. Memb. Sci.* **2009**, *331* (1), 143–151. https://doi.org/https://doi.org/10.1016/j.memsci.2009.01.027.

(70) Connolly, M. L. Analytical Molecular Surface Calculation. *J. Appl. Crystallogr.* **1983**, *16* (5), 548–558. https://doi.org/10.1107/S0021889883010985.

(71) Sun, T.; Fang, M.; Wu, Z.; Yu, L.; Li, J. Molecular Dynamics Insights into the Structural and Diffusive Properties of ZIF-8/PDMS Mixed Matrix Membranes in the n-Butanol/Water Pervaporation Process. *Model. Simul. Mater. Sci. Eng.* **2017**, *25* (3), 35002. https://doi.org/10.1088/1361-651x/aa584f.

(72) Wang, Y.; Wei, Q.; Wang, S.; Chai, W.; Zhang, Y. Structural and Water Diffusion of Poly(Acryl Amide)/Poly(Vinyl Alcohol) Blend Films: Experiment and Molecular Dynamics Simulations. *J. Mol. Graph. Model.* **2017**, *71*, 40–49. https://doi.org/https://doi.org/10.1016/j.jmgm.2016.11.001.